Draft version April 16, 2010
Preprint typeset using LaTeX style emulateapj v. 6/22/04

ON THE STELLAR CONTENT OF THE CARINA DWARF SPHEROIDAL GALAXY[1]

G. Bono[2,3], P. B. Stetson[4,18], A. R. Walker[5], M. Monelli[6], M. Fabrizio[2], A. Pietrinferni[7], E. Brocato[7], R. Buonanno[2,8], F. Caputo[3], S. Cassisi[7], M. Castellani[3], M. Cignoni[9,10], C. E. Corsi[3], M. Dall'Ora[11], S. Degl'Innocenti[12,13], P. François[14], I. Ferraro[3], G. Iannicola[3], M. Nonino[15], P. G. Prada Moroni[12,13], L. Pulone[3], H. A. Smith[16], F. Thevenin[17]

(Dated: drafted April 16, 2010 / Received / Accepted)
Draft version April 16, 2010

ABSTRACT

We present deep, accurate and homogeneous multiband optical (U,B,V,I) photometry of the Carina dwarf spheroidal galaxy, based on more than 4,000 individual CCD images from three different ground-based telescopes. Special attention was given to the photometric calibration, and the precision for the B, V, and Ibands is generally better than 0.01 mag. We have performed detailed comparisons in the V, B–V and V, B–I color-magnitude diagrams (CMDs) between Carina and three old, metal-poor Galactic Globular Clusters (GGCs, M53, M55, M79). We find that only the more metal-poor GCs (M55, [Fe/H]=–1.85; M53, [Fe/H]=–2.02 dex) provide a good match with the Carina giant branch. We have performed a similar comparison in the V, V–I CMD with three intermediate-age clusters (IACs) of the Small Magellanic Cloud (Kron 3, NGC 339, Lindsay 38). We find that the color extent of the SGB of the two more metal-rich IACs (Kron 3, [Fe/H]=–1.08; NGC339, [Fe/H]=–1.36 dex) is smaller than the range among Carina's intermediate-age stars. Moreover, the slope of the RGB of these two IACs is shallower than the slope of the Carina RGB. However, the ridge line of the more metal-poor IAC (Lindsay 38, [Fe/H]=–1.59 dex) agrees quite well with the Carina intermediate-age stars. These findings indicate that Carina's old stellar population is metal-poor and appears to have a limited spread in metallicity (Δ[Fe/H]=0.2–0.3 dex). The Carina's intermediate-age stellar population can hardly be more metal-rich than Lindsay 38 and its spread in metallicity also appears modest. We also find that the synthetic CMD constructed assuming a metallicity spread of 0.5 dex for the intermediate-age stellar component predicts evolutionary features not supported by observations. In particular, red clump stars should attain colors that are redder than red giant stars, but this is not seen. The above results are at odds with recent spectroscopic investigations suggesting that Carina stars cover a broad range in metallicity (Δ[Fe/H]$\sim$1–2 dex). We also present a new method to estimate the metallicity of complex stellar systems using the difference in color between the red clump and the middle of the RR Lyrae instability strip. The observed colors of Carina's evolved stars indicate a metallicity of [Fe/H]=–1.70$\pm$0.19 dex, which agrees quite well with spectroscopic measurements.

Subject headings: galaxies: dwarf — galaxies: stellar content — stars: evolution — stars: fundamental parameters

1. INTRODUCTION

Dwarf galaxies play a fundamental role in several astrophysical problems. Current cosmological simulations predict dwarf satellite populations significantly larger than the number of dwarfs observed near giant spirals like the Milky Way and M31. This discrepancy is called the "missing satellite problem" and is a challenge to the currently most popular cosmological model: the Λ Cold Dark Matter paradigm (Klypin et al. 1999; Moore et al. 2006; Madau et al. 2008). However, it has not yet been established whether this discrepancy is due to limitations in the theoretical modeling or to observational bias at the faint end of the dwarf galaxy luminosity function (Klimentowski et al. 2009; Koposov et al. 2009; Kravtsov 2010).

Moreover, detailed analyses of the distribution of dwarf galaxies in multi-dimensional parameter space indicate that they follow very tight relations. In particular, Prada

[1] Based on images collected with the MOSAICII camera available at the CTIO 4m Blanco telescope, La Serena; (2003B-0051, 2004B-0227, 2005B-0092, P.I.: A.R. Walker) and in part with the WFI available at the 2.2m MPG/ESO telescope (A064.L-0327) and with images obtained from the ESO/ST-ECF Science Archive Facility.

[2] Dipartimento di Fisica, Università di Roma Tor Vergata, via della Ricerca Scientifica 1, 00133 Rome, Italy; bono@roma2.infn.it
[3] INAF–OAR, via Frascati 33, Monte Porzio Catone, Rome, Italy
[4] DAO–HIA, NRC, 5071 West Saanich Road, Victoria, BC V9E 2E7, Canada
[5] NOAO–CTIO, Casilla 603, La Serena, Chile
[6] IAC, Calle Via Lactea, E38200 La Laguna, Tenerife, Spain
[7] INAF–OACTe, via M. Maggini, 64100 Teramo, Italy
[8] ASI–Science Data Center, ASDC c/o ESRIN, via G. Galilei, 00044 Frascati, Italy
[9] Dipartimento di Astronomia, Università di Bologna, via Ranzani 1, 40127 Bologna, Italy
[10] INAF–OAB, via Ranzani 1, 40127 Bologna, Italy
[11] INAF–OACN, via Moiariello 16, 80131 Napoli, Italy
[12] Dept. of Physics, Univ. Pisa, Largo B. Pontecorvo 2, 56127 Pisa, Italy
[13] INFN, Sez. Pisa, via E. Fermi 2, 56127 Pisa, Italy
[14] Observatoire de Paris-Meudon, GEPI, 61 avenue de l'Observatoire, 75014 Paris, France
[15] INAF–OAT, via G.B. Tiepolo 11, 40131 Trieste, Italy
[16] Dept. of Physics and Astron. Michigan State University, East Landsing, MI 48824, USA
[17] Observatoire de la Cote d'Azur, BP 4229, 06304 Nice, France
[18] Visiting Astronomer, Cerro Tololo Inter-American Observatory, National Optical Astronomy Observatories, operated by AURA, Inc., under cooperative agreement with the NSF.

& Burkert (2002) suggested that Local Group (LG) dwarf galaxies show strong correlations (Fundamental Line - FL) among mass-to-light (M/L) ratio, surface brightness, and metallicity. They explained the correlation between M/L ratio and metallicity using a simple chemical enrichment model in which the hot metal-enriched gas, at the end of the star-formation epoch, is lost via continuous galactic winds (Mac Low & Ferrara 1999). In a recent investigation Woo & Chiueh (2009) reached similar conclusion, i.e., LG dwarf galaxies follow a one-parameter relation driven by the total stellar mass. They also found that dwarf spheroidals (dSphs) appear to be, at fixed stellar mass, systematically more metal-rich than dwarf irregulars (dIs, see also Mateo (1998)). Futhermore, the FL of dIs in a five-dimensional parameter (total space mass, surface brightness, rotation velocity, metallicity, star formation rate) is linear and tight, and extends the scaling relations of giant late-type galaxies into the low-mass regime. On the other hand, the FL of dSphs as defined in a four-dimensional parameter space (total mass, surface brightness, rotation velocity, metallicity) is also linear and very tight, but it does *not* lie on an extrapolation of the scaling relations of giant early-type galaxies. Iron and heavy-element abundances, the spread in these quantities, and the star-formation history (SFH) of LG dwarf galaxies, are crucial observational constraints on the physical mechanisms responsible for the scaling relations described above, and on their implications for different cosmological models (Orban et al. 2008). Spectroscopic investigations based on high-resolution spectra of bright red giants (RGs) in several LG dSphs indicate a large spread in iron abundance (Shetrone et al. 2001, 2003). This is also supported by metallicity estimates from the CaII triplet method (Battaglia et al. 2008). In this context, the Carina dSph is particularly relevant: (*i*) It is relatively close and its central density is modest (ρ=0.17$M_\odot/pc^3$, Mateo (1998)) so it is easily resolved with ground-based telescopes (Mould & Aaronson 1983). (*ii*) It is *the* LG dSph most clearly showing multiple, widely separated star formation episodes(Mighell (1990, 1997); Smecker-Hane et al. (1994, 1996); Hurley-Keller et al. (1998); Hernandez et al. (2000); Harbeck et al. (2001); Dolphin (2002); Rizzi et al. (2003)) with a tail that might extend to less than one Gyr ago (Monelli et al. (2003)). (*iii*) It is also a benchmark to constrain the pulsation properties of old (RR Lyrae, Saha et al. (1986)) and intermediate-age (dwarf Cepheids, Mateo et al. (1998); Anomalous Cepheids, Dall'Ora et al. (2003)) variable stars. (*iv*) High-resolution spectra are available for a sample of ten bright RGs. The mean metallicity is [Fe/H]=–1.69 with σ=0.51 dex (Koch et al. 2008). Independent measurements by Shetrone et al. (2003), using high resolution spectra for five bright RGs, provided a mean metallicity of [Fe/H]=–1.64 and σ=0.2 dex. (*iv*) Medium-resolution calcium triplet measurements are also available for a large sample (437) of RG stars (Koch et al. 2006); their metallicity distribution shows a peak at [Fe/H]=–1.72±0.01 (metallicity scale by Carretta & Gratton 1997) and the metallicity ranges from ∼–2.5 to ∼–0.5 dex. Using the same spectra, but different selection criteria (364 candidate Carina stars), Helmi et al. (2006) found the same peak in the metallicity distribution ([Fe/H]=–1.7±0.1 dex) and metallicities ranging from ∼–2.3 to ∼–1.3 dex (see their Fig. 2).

Deep, accurate photometric investigations indicate an old (13 Gyr) stellar population and several distinct intermediate-age populations (2–6 Gyr) together with a blue plume of younger stars. The occurrence of both old and intermediate-age populations is also indicated by two distinct samples of core helium burning stars: an old, wide HB and a separate red clump (RC). The shape and thickness of the RGB (ΔB–$V\sim$0.02 for 20.5$\lesssim V \lesssim$20.75 mag) suggest that the old and intermediate-age stellar populations have a minimal spread in chemical composition. This seems inconsistent with the spectroscopic observations that indicate a metallicity distribution possibly reaching extreme values near –3.1 and +0.1 dex (Zinn & West 1984, scale), or near –2.8 and –0.2 dex (Carretta & Gratton 1997, scale).

Despite the criticisms raised by Koch et al. (2006), conclusions based on purely photometric indicators are hampered by only two major factors: (*i*) A decrease in photometric precision when moving from bright to faint RG stars might produce a spread in color mimicking a spread in metal content. In particular, Carina's stellar density is very low, requiring that photometry be obtained with multi-chip CCD cameras or with many different pointings of a single CCD. A high degree of consistency in the photometric zero-points across the field is essential to avoid spurious broadening of the RG and Main Sequence (MS) loci. (*ii*) Due to its low surface density, large extent, and low Galactic latitude (–22°), the Carina sample is contaminated by foreground field stars. Their colors, unfortunately, are similar to the Carina RGB, once again mimicking a broadening in color due to a spread in age/metallicity.

Our group is involved on a long-term investigation of the stellar populations in the Carina dSph. In particular, we have assembled our own and archival *UBVI* images covering the entire body of the galaxy. In this investigation we focus on comparing Carina with old and intermediate-age template clusters. We also present a new method for estimating the metal content of complex stellar systems from the difference in color between the middle of the RR Lyrae instability strip and the peak of RC stars.

2. OBSERVATIONS AND DATA REDUCTION

The data were collected in various observing runs between 1992 December and 2005 January. They include images from three telescopes: the CTIO 1.5m telescope with a single Tektronix2K CCD, the CTIO 4m Blanco telescope with the MosaicII camera, and the ESO/MPG 2.2m telescope with the Wide Field Imager camera (both proprietary and archival data). Details of the observations will be presented in a future paper. The data presented here represent 4,152 individual CCD images with essentially complete coverage of the central regions of Carina ($\approx 40' \times 55'$, lacking only those regions obliterated by bright foreground stars), and some sampling of the galaxy's halo out to an extreme radius of $\sim$108′. They were obtained in four photometric bands (B and I with the 1.5m telescope, and $UBVI$ with both the 4m and 2.2m telescopes).

The data were reduced using the DAOPHOT/ALLFRAME package (Stetson 1987, 1994). Individual PSFs were produced for each chip of every exposure, using semi-automated routines to

select bright, isolated PSF stars. Subsets of the data from each observing run were first reduced separately. Finally, everything was merged together and a single run of ALLFRAME was adopted to reduce all the images of the center of Carina, with separate reductions for non-overlapping outlying fields. Because of the multiple chips and pointings required to cover the galaxy, no star appears in every image; any given star may have up to 17 calibrated measurements in U, 156 in B, 207 in V, and 70 in I. A total of 205,338 individual stars were catalogued and measured. Among these, 72,595 have photometric measurements in all four filters, and 129,230 have at least V and either B–V or V–I. The remainder, either extremely faint or located near the periphery of our coverage, have astrometry and instrumental magnitudes only.

The Carina data were contained within 206 individual datasets, where a dataset is essentially the totality of data obtained with one CCD from one night of observing. These, along with 1,331 datasets from other nights and other telescopes, were calibrated to the current version of Stetson's (2000) photometric standard system, which is believed to be equivalent to that of (Landolt 1992) to well under 0.01 mag in each of B, V, and I (see also Stetson (2005)). The U photometric bandpass is more problematic, and in this paper we will employ the U-band data only for qualitative and relative comparisons.

3. RESULTS AND DISCUSSIONS

For a robust discrimination of candidate Carina members from foreground field stars and background galaxies we adopted the U–V,B–I color-color diagram (C-CD). The top panel of Fig. 1 shows that this is effective for distinguishing candidate Carina and field stars. Carina RGs (U–$V\geq0.6$, B–$I\geq1.4$) attain, at fixed B–I, bluer U–V colors than field stars. The difference is mainly caused by a difference in the mean metallicity between Carina and the more metal-rich Galactic disk stars, but the difference in surface gravity between galaxy giants and foreground dwarfs may also play a role. In contrast, hot horizontal-branch (HB) stars and relatively young MS stars in Carina (B–$I\lesssim0.4$) are relatively free from field star contamination, since they are bluer than the thick disk and halo turnoffs; compact background galaxies represent the principal source of contamination among these bluer objects. Fortunately, this C-CD is also a good diagnostic to separate candidate Carina stars from blue background galaxies since the latter show, at fixed B–I, systematically bluer U–V colors than stars of any luminosity class or metallicity (apart from white dwarfs, which are not an issue here).

Based on the above empirical evidence, we performed a series of tests to identify candidate Carina stars using various color-magnitude diagrams (CMDs) together with the C-CD. The solid-outlined box in the top panel of Fig. 1 shows the final selection, while the bottom panels show the V,B–V CMD of the total sample (left), the candidate Carina stars (middle), and the candidate non-member objects (right). Note that after the selection there remain some field stars with colors similar to Carina's RGB ($V\leq21.5$, B–$V\sim$0.4-0.6; middle panel). However, RG stars are distributed along a very narrow sequence over the entire magnitude range ($18\leq V\leq23$), and the number of field stars lying near that RGB in both color and magnitude is appreciably reduced. The same statement applies to the intermediate-age red clump (RC: $V\sim20.5$, B–$V\sim0.65$) and to the old HB ($V\sim20.75$, B–$V\sim0.65$). These evolutionary phases are characterized by very narrow distributions in either magnitude or color or both. The improvement compared to data already available in the literature is due to smaller photometric uncertainties ($\sigma_{B-V}\leq0.02$ for $V\leq21$, see error bars in Fig. 1). Plain evolutionary arguments (Monelli et al. 2003; Zoccali et al. 2003) suggest that small dispersions in magnitude and color in these evolutionary phases imply a negligible spread in chemical composition. This finding supports the results based on B,V,I photometry of Carina RG stars obtained by Rizzi et al. (2003). The presence of a few stars in the right panel with magnitudes and colors typical of red HB ($V\sim20.75$, B–$V\sim0.4$) and faint subgiant branch (SGB) stars ($V\sim23$, B–$V\sim0.5$) demonstrates that our C-CD selection is imperfect—especially at intermediate colors—and some real Carina members have probably been erroneously rejected. However, in these photometric selections it is more important to keep probable non-members out than to keep possible members in (Calamida et al. 2009).

To provide robust constraints on Carina's stellar content, we compared it with stellar systems characterized by different ages and metal abundances. In particular, to constrain the old stellar population we selected three globular clusters (GCs)—M79 = NGC 1904, M55 = NGC 6809, and M53 = NGC 5024—with metal abundances ranging from –1.64±0.15 to –2.02±0.15, and low foreground reddenings (E(B–V)$\leq$0.09, see Table 1). The optical BVI photometry of these GCs is also on the Stetson (2005) system. The accuracy of the photometry is certainly better than our knowledge of the foreground reddening toward these clusters and Carina. The V, B–V (left panels) and V, B–I (middle panels) CMDs of the selected GCs are shown in Fig. 2, together with their individual ridge lines (red curves). We also selected three intermediate-age clusters (IACs) belonging to the Small Magellanic Cloud (SMC)—Kron 3, NGC 339, Lindsay 38—with similar ages and iron contents ranging from –1.08±0.12 to –1.59±0.10 dex (Glatt et al. 2009, see Table 1). The photometry for these clusters is from ACS@HST data transformed into the V, I Johnson-Cousins bands using relations by Siranni et al. (2005). These clusters are *not* included in the homogenous photometry project (the original sources of the data are listed in Table 1), so we are unable to independently confirm the precision of the photometry or the accuracy of the calibrations. Data plotted in the right panels of Fig. 2 display the V,V–I CMDs for these clusters together with their ridge lines and the outlines of their RCs.

To compare the GCs with the old stellar populations in Carina, we arbitrarily shifted their ridge lines in magnitude and color to provide a good fit with the SGB ($23.25\lesssim V\lesssim23.75$, $0.45\leq B$–$V\leq0.60$) in Carina. Then we inferred the difference in distance and in reddening between Carina (μ=20.15, E(B–V)=0.03; Dall'Ora et al. (2003); Pietrzynski et al. (2009)) and the individual GCs. The distances and the cluster reddenings we found following this approach agree, within the errors, with similar estimates available in the literature (see columns 4

and 5 in Table 1). The top and the middle left panels of Fig. 3 show that the GCs M79 and M55 provide a poor match to Carina, since hot HB stars are systematically brighter than Carina HB stars. On the other hand, both the GB and the HB of the more metal-poor GC (M53) match Carina quite well. The same outcomes apply if the comparison is performed using the V, B–I CMDs (see the middle panels in Fig. 3). The extinction in the BVI bands was estimated using the empirical relations provided by McCall (2004).

The same approach was followed to compare the IACs with Carina stellar populations. The ridge lines were shifted in magnitude and color to provide a good fit to the lower envelope of intermediate-age SGB ($22.5 \lesssim V \lesssim 23.0$, $0.45 \lesssim V$–$I \lesssim 0.80$) stars in Carina. The distances that we estimate are larger than those estimated by Glatt et al. (2009) (see Table 1) using isochrones. However, the current distances agree, within the errors, with SMC distances available in the literature (Romaniello et al. 2009). The same outcome applies for the cluster reddenings (see the right panels in Fig. 3). This comparison between Carina and the IACs revealed the following: (i) the color extents of the SGBs of the the two more metal-rich clusters (Kron 3 and NGC 339; i.e., the length of the horizontal sequence between the upper MS and the lower GB) are smaller than the color range covered by Carina's intermediate-age SGB stars; (ii) the slope of the RGB in the two more metal-rich clusters (Kron 3, NGC 339) is shallower than the observed slope of Carina's RGB; (iii) the ridge line of Lindsay 38 is a fairly good match to Carina's intermediate-age population. (iv) the RC contour of Kron 3 agrees with Carina's RC, while for the other two clusters the clumps are either slightly redder and brighter (NGC 339) or marginally fainter (Lindsay 38).

These comparisons indicate that Carina's old population is relatively metal-poor, and its spread in metallicity is modest: at most 0.2–0.3 dex. Carina's intermediate-age population seems to have the same metallicity as Lindsay 38, or perhaps slightly lower. The spread in metal abundance in this stellar component also seems very limited, since the RGBs of the two more metal-rich IACs are considerably redder than the red envelope of Carina's RGB. The lack of accurate photometry for metal-poor ([Fe/H]<–1.6 dex) IACs with well populated RGBs prevents us from providing more firm constraints on Carina's intermediate-age population. These findings do not depend on the adopted metallicity scale, and if we adopt instead iron abundances on the Carretta et al. (2009) metallicity scale (see column 3 in Table 1), the metallicity range inferred for Carina is very similar.

For a new estimate of the metal abundance of Carina we decided to use a new indicator. Evolutionary prescriptions for old and intermediate-age stellar structures indicate that the difference in color between the center of the RR Lyrae instability strip and the RC stars is strongly correlated with iron abundance. The correlation is caused by the mild dependence of the color of the instability strip on iron abundance and by the significant dependence of the color of RC stars when moving from metal-poor to metal-rich compositions (see Fig. 4). We estimated the predicted difference in color between RC stars (at the beginning of central helium burning) and the center of RR Lyrae strip ($\log T_e$=3.85) from the large set of scaled-solar evolutionary models (Pietrinferni et al. 2004) available in the BaSTI database[19]. We adopted evolutionary prescriptions that cover a wide range of iron abundances (–2.27≤[Fe/H]≤+0.06 dex), and an age range of 1–6 Gyr for the intermediate-age population and 13 Gyr for the old population. Note that the instability strip is minimally affected by cluster age when moving from 7–8 to 12–13 Gyr. In this context two robust evolutionary predictions need to be underlined. (i) When moving from metal-poor to metal-rich compositions, the intermediate-age RC becomes redder than the old RGB for [Fe/H]=–1.79 dex (see the top panel of Fig. 4). Current evolutionary models predict that a change in metallicity from [Fe/H]=–1.96 to [Fe/H]=–1.49 produces a change in V magnitude of RC stars of 0.03 mag, but a change of 0.12 mag in the B–V color. (ii) The spread in magnitude of HB stars at the mean color of the RR Lyrae strip increases, as expected, with the spread in metallicity. Note that a change in metallicity from [Fe/H]=–1.96 to [Fe/H]=–1.49 implies a change in V magnitude of HB stars of 0.10 mag, but a change smaller than 0.01 mag in the B–V color of the instability strip (see the bottom panel of Fig. 4).

Finally, we performed a linear regression between metallicity and the RC–HB difference in three different colors:

$$[Fe/H] = (-3.02 \pm 0.03) + (3.89 \pm 0.05)\Delta(B\text{–}V)^{RC}_{HB}$$
$$[Fe/H] = (-3.47 \pm 0.04) + (2.37 \pm 0.04)\Delta(B\text{–}I)^{RC}_{HB}$$
$$[Fe/H] = (-4.13 \pm 0.08) + (6.02 \pm 0.15)\Delta(V\text{–}I)^{RC}_{HB}$$

The above relations (see also right panels in Fig. 5) indicate that the difference in the B–I color is significantly more sensitive to [Fe/H] than the B–V color. The V–I is the least sensitive of all and shows a stronger nonlinear trend in the metal-poor ([Fe/H]≤–1.5) regime. We estimated the difference in color between the RC and the middle of the RR Lyrae instability strip (see the left panels in Fig. 5). We found $\Delta B\text{–}V^{RC}_{HB}$=0.37±0.05, $\Delta B\text{–}I^{RC}_{HB}$=0.75±0.05 and $\Delta V\text{–}I^{RC}_{HB}$=0.40±0.05 mag, where the errors account for uncertainties in the photometry and in the estimate of the mean color of the RR Lyrae strip. We applied the above relations and we found the following mean metallicities: [Fe/H]=–1.60±0.24($\Delta B\text{–}V^{RC}_{HB}$), [Fe/H]=–1.70±0.19($\Delta B\text{–}I^{RC}_{HB}$) and [Fe/H]=–1.76±0.44($\Delta V\text{–}I^{RC}_{HB}$). We adopted the estimate based on B–I, since it is the most precise.

As a further test to constrain the spread in metallicity of the Carina sub-populations, we computed a series of synthetic CMDs changing the spread both in age and in metal content. The set of evolutionary models used for these numerical simulations are the same used to derive the new metallicity indicator (Pietrinferni et al. 2004). The code adopted to compute the synthetic CMDs has already been discussed by Pietrinferni et al. (2004) and by Cordier et al. (2007). We only briefly mention the initial parameters adopted to compute the synthetic CMDs. The Initial Mass Function was modeled using a power law with a Salpeter exponent (α=-2.35), and we assumed a fraction of unresolved binaries of the order of 10% with a minimum mass ratio for the binary systems equal to 0.7. The synthetic CMDs were constructed assuming two star formation events, with a

[19] Evolutionary models can be download from http://www.oa-teramo.inaf.it/BASTI

mean age of 2.5–4 Gyr for the intermediate-mass and of 11–13 Gyr for the low-mass sub-population (Monelli et al. 2003). We also assumed that the two star formation episodes include the same fraction of stars. Moreover, we assumed mean metallicities of [Fe/H]=–1.5 and of –2.0 dex for the intermediate-age and the old burst, respectively. In accordance with the above findings, we assumed the same spread in metallicity—±0.1 dex—for the intermediate and the old star formation episode. Finally, to mimic actual observations, synthetic photometric errors were added using a Gaussian in the B and V bands with a dispersion equal to 0.02 mag. The above assumptions adopted to simulate the Carina observations are crude, but a detailed analysis is beyond the aims of this investigation. We plan to study the Carina star formation history in a forthcoming paper (Monelli et al. 2010). Data plotted in the top panel of Fig. 6 show that the aforementioned assumptions provide evolutionary features that are in reasonable agreement with the observations (see Fig. 2). In particular, both RC and HB stars are clearly separated in magnitude and in color from each other and from RG stars. Moreover, we selected two bins along the RGB for $20.75 \leq m_v \leq 21.25$ and $21.50 \leq m_v \leq 22.00$ and we found that the spread in B–V color is ∼0.06 mag. This value is quite similar, within the errors, to the spread in B–V color of the observed CMD at the same magnitude intervals, i.e., 0.06 mag. To constrain the impact of a spread in metal content, we used the same evolutionary ingredients adopted to construct the above synthetic CMD, but we assumed for each of the two stellar components a spread in metallicity of 0.2 dex. The spread in B–V color at the same magnitude intervals is slightly larger than observed, namely 0.08 mag.

Finally, we adopted for the intermediate-age stellar component alone a spread in metallicity of 0.5 dex. Data plotted in the bottom panel of Fig. 6 clearly show that such a spread in metallicity causes the RC stars to attain colors that are redder than the RG stars. The spread in B–V color at the same magnitude intervals is a factor of two larger than observed, i.e., 0.12 mag. Moreover, the synthetic CMD suggests the occurrence of subgiant and giant branch stars with colors that are redder than the subgiant of the old sub-population. The observed CMD does not show these features.

The comparison with empirical calibrators further supports the contention that Carina hosts predominantly metal-poor stellar populations, in agreement with the spectroscopic investigations. However, the limited range in color covered by the RC stars appears incompatible with the spectroscopic results: the spread in iron abundance of the intermediate-age population is either small, or is counterbalanced by some other—as yet unrecognized—variable. The same conclusion applies for the old population, based on the limited magnitude spread among the old HB stars. These conclusions are also supported by synthetic CMDs constructed assuming a different spread in metallicity between the intermediate and the old sub-populations. The simulations indicate a spread in metallicity of the two sub-populations smaller than 0.2 dex.

It is a real pleasure to thank an anonymous referee for his/her positive comments on the results of this investigation and for his/her suggestion. We also thank A. Grazian, for several useful discussions concerning the intrinsic color of galaxies as a function of the redshift and K. Glatt for sending us her photometric catalogs of the three SMC clusters. This project was supported by Monte dei Paschi di Siena (P.I.: S. Degl'Innocenti), PRIN-INAF2006 (P.I.: M. Bellazzini). HAS thanks the National Science Foundation for support under grant AST0607249.

REFERENCES

Battaglia, G., Irwin, M., Tolstoy, E., Hill, V., Helmi, A., Letarte, B.,& Jablonka, P. 2008, MNRAS, 383, 183
Calamida, A. et al. 2009, ApJ, 706, 1277
Carretta, E. & Gratton, R. G. 1997 A&AS, 121, 95 (CG97)
Carretta, E., Bragaglia, A., Gratton, R., D'Orazi, V., & Lucatello, S. 2009, A&A, 508, 695 (C09)
Castellani, V., Cignoni, M., Degl'Innocenti, S., Petroni, S., PradaMoroni, P. G. 2002, MNRAS, 334, 69
Cordier, D., Pietrinferni, A., Cassisi, S., & Salaris, M. 2007, AJ, 133, 468
Da Costa, G. S. & Hatzidimitriou D. 1998, AJ, 115, 1934
Dall'Ora, M. et al. 2003, AJ, 126, 197
Dékány, I., & Kovács, G. 2009, A&A, 507, 803
Dolphin, A. E. 2002, MNRAS, 332, 91
Dotter, A., Chaboyer, B., Ferguson, J. W., Lee, H.-c., Worthey, G., Jevremović, D., & Baron, E. 2007, ApJ, 666, 403
Ferraro, F. R., Messineo, M., Fusi Pecci, F., de Palo, M. A., Straniero, O., Chieffi, A., & Limongi, M. 1999, AJ, 118, 1738
Glatt, K. et al. 2009, AJ, 138, 1403
Harbeck, D., et al. 2001, AJ, 122, 3092
Helmi, A., et al. 2006, ApJ, 651, L121
Hernandez, X., Gilmore, G., & Valls-Gabaud, D. 2000, MNRAS, 317, 831
Hurley-Keller, D., Mateo, M., & Nemec, J. 1998, AJ, 115, 1840
Kayser, A., Grebel, E. K., Harbeck, D. R., Cole, A. A., Koch, A., Glatt, K., Gallagher, J. S., & da Costa, G. S. 2007, in IAUS 241, Stellar populations as Building Blocks of Galaxies, ed. A. Vazdekis, & R.F. Peletier (Cambridge: Cambridge University Press), 351
Klimentowski, J., Łokas, E. L., Kazantzidis, S., Mayer, L., Mamon, G. A., & Prada, F. 2009, MNRAS, 400, 2162
Klypin, A., Kravtsov, A. V., Valenzuela, O., & Prada, F. 1999, ApJ, 522, 82
Koch, A., Grebel, E. K., Wyse, R. F. G., Kleyna, J. T., Wilkinson, M. I., Harbeck, D. R., Gilmore, G. F., & Evans, N. W. 2006, AJ, 131, 895
Koch, A., Grebel, E. K., Gilmore, G. F., Wyse, R. F. G., Kleyna, J. T., Harbeck, D. R., Wilkinson, M. I., & Wyn Evans, N. 2008, AJ, 135, 1580
Koposov, S. E., Yoo, J., Rix, H.-W., Weinberg, D. H., Macciò, A. V., & Escudé, J. M. 2009, ApJ, 696, 2179
Kraft, R. P., & Ivans, I. I. 2004, Origin and Evolution of the Elements, ed. A. McWilliam and M. Rauch (Pasadena: Carnegie Observatories), 33 (KI04)
Kravtsov, A. 2010, AdAst, 1
Landolt, A. U. 1992, AJ, 104, 340
Mac Low, M. & Ferrara, A. 1999, ApJ, 513, 142
McCall, M. L. 2004, AJ, 128, 2144
Madau, P., Diemand, J., & Kuhlen, M. 2008, ApJ, 679, 1260
Mateo, M. L. 1998, ARA&A, 36, 435
Mateo, M., Hurley-Keller, D., & Nemec, J. 1998, AJ, 115, 1856
Mighell, K. J. 1990, A&AS, 82, 1
Mighell, K. J. 1997, AJ, 114, 1458
Monelli, M. et al. 2003, AJ, 126, 218
Moore, B., Diemand, J., Madau, P., Zemp, M., & Stadel, J. 2006, MNRAS, 368, 563
Mould, J., & Aaronson, M. 1983, ApJ, 273, 530
Orban, C., Gnedin, O. Y., Weisz, D. R., Skillman, E. D., Dolphin, A. E., & Holtzman, J. A. 2008, ApJ, 686, 1030

TABLE 1
Intrinsic parameters of old and intermediate-age calibrating clusters.

Name	[Fe/H]	[Fe/H][c]	μ	E($B-V$)	Age
NGC 1904 - M79	-1.64±0.10[a]	-1.58±0.02	15.61±0.10[d]	0.01±0.02[d]	12.6±1.3[f]
NGC 6809 - M55	-1.85±0.10[a]	-1.93±0.02	13.69±0.10[d]	0.09±0.02[d]	12.4±1.7[f]
NGC 5024 - M53	-2.02±0.15[a]	-2.06±0.09	16.24±0.10[d]	0.01±0.02[d]	11.2±1.8[f]
Kron 3	-1.08±0.12[b]	-0.97±0.14	18.83[e]	0.006[e]	6.3[e]
NGC 339	-1.36±0.16[b]	-1.25±0.18	18.75[e]	0.04[e]	6.0[e]
Lindsay 38	-1.59±0.10[b]	-1.52±0.12	19.00[e]	0.04[e]	6.5[e]

[a]Iron abundance by Kraft & Ivans (2004).
[b]Iron abundance in the ZW84 metallicity scale by Da Costa & Hatzidimitriou (1998, Kron 3, NGC 339) and Kayser et al. (2007, Lindasy 38).
[c]Iron abundance by C09.
[d]Distance modulus and reddening by Ferraro et al. (1999, M79), Vargas et al. (2007, M55) and Dékány & Kovács (2009, M53). The uncertainty on distance and reddening are 5% and 20%.
[e]Distance modulus, reddening and age by Glatt et al. (2009) using cluster isochrones by Dotter et al. (2007).
[f]Cluster ages: Salaris & Weiss (2002, M79, M55), Sarajedini (2009, M53).

Pietrinferni, A., Cassisi, S., Salaris, M., & Castelli, F. 2004, ApJ, 612, 168
Pietrzyński, G., Górski, M., Gieren, W., Ivanov, V. D., Bresolin, F., & Kudritzki, R.-P. 2009, AJ, 138, 459
Prada, F. & Burkert, A. 2002, ApJ, 564L, 73
Rizzi, L., Held, E. V., Bertelli, G., & Saviane, I. 2003, ApJ, 589, L85
Rocca-Volmerange, B., Tsalmantza, P., & Kontizas, M. 2008, SF2A-2008, 33
Romaniello, M., et al. 2009, American Institute of Physics Conference Series, 1170, 99
Saha, A., Monet, D. G., & Seitzer, P. 1986, AJ, 92, 302
Salaris, M., & Weiss, A. 2002, A&A, 388, 492
Sarajedini, A. 2009, in IAUS 258, The Ages of Stars 2009, ed. E.E. Mamajek, D.R. Soberblom, & R.F.G. Wyse (Cambridge: Cambridge University Press), 221
Shetrone, M. D., Côté, P., & Sargent, W. L. W. 2001, ApJ, 548, 592
Shetrone, M., Venn, K. A., Tolstoy, E., Primas, F., Hill, V., & Kaufer, A. 2003, AJ, 125, 684
Sirianni, M. et al. 2005, PASP, 117, 1049
Smecker-Hane, T. A., Stetson, P. B., Hesser, J. E., & Lehnert, M. D. 1994, AJ, 108, 507
Smecker-Hane, T. A., Stetson, P. B., Hesser, J. E., & Vandenberg, D. A. 1996, in ASP Conf. Ser. 98, The Impact of Stellar Physics on Galaxy Evolution, ed. C. Leitherer, U. Fritze-von Alvensleben, & J. Huchra (San Francisco: ASP), 328
Stetson, P. B. 1987, PASP, 99, 191
Stetson, P. B. 1994, PASP, 106, 250
Stetson, P. B. 2000, PASP, 112, 925
Stetson, P. B. 2005, PASP, 117, 563
Vargas Álvarez, C. A., & Sandquist, E. L. 2007, AJ, 134, 825
Woo, T. & Chiueh, T. 2009, ApJ, 697, 850
Zinn, R. & West, M. J. 1984, ApJS, 55, 45 (ZW84)
Zoccali, M. et al. 2003, A&A, 399, 931

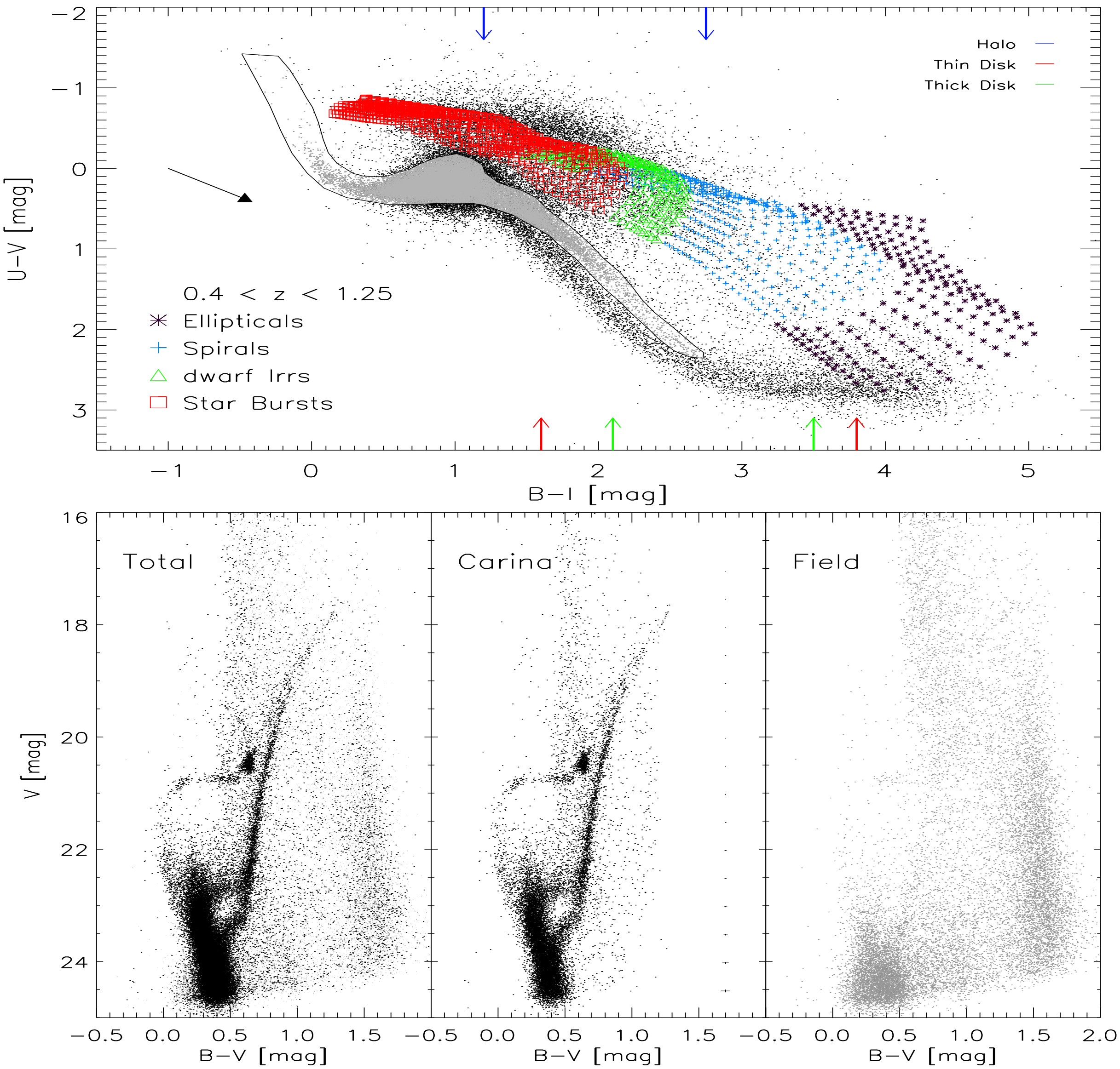

FIG. 1.— Top – U–V, B–I Color-Color Diagram (C-CD) of Carina dSph. The curved box encloses candidate Carina stars (grey dots). The black dots represent probable field objects. Predicted distributions (Rocca-Volmerange et al. 2008) of elliptical (asterisks), spiral (pluses), SB (triangles), irregular and star burst (squares) galaxies as a function of the redshift are also showed. The vertical colored arrows mark the predicted (Castellani et al. 2002) peaks in B–V color for the halo (blue), the thick disk (green) and the thin disk (red). The black arrow shows the reddening vector. Bottom – Left – V, B–V Color-Magnitude Diagram (CMD) of Carina dSph. Bottom – Middle – V, B–V CMD of candidate field stars according to the C-CD selection. The error bars on the right represent the intrinsic photometric error in magnitude and in color. Rejection of thick-disk turnoff stars is obviously imperfect near B–I∼0.5, where the C-CD loses discriminating power. Bottom – Right – V,B–V CMD of candidate Carina stars according to the C-CD selection. A hint of the Carina HB near V≈20.75 and of the SGB at $22.5 \lesssim V \lesssim 23.75$ confirm that discrimination is imperfect at these intermediate colors. The block of dots with B–I<0.5, V>23.5 is probably dominated by background galaxies rather than Carina turnoff stars.

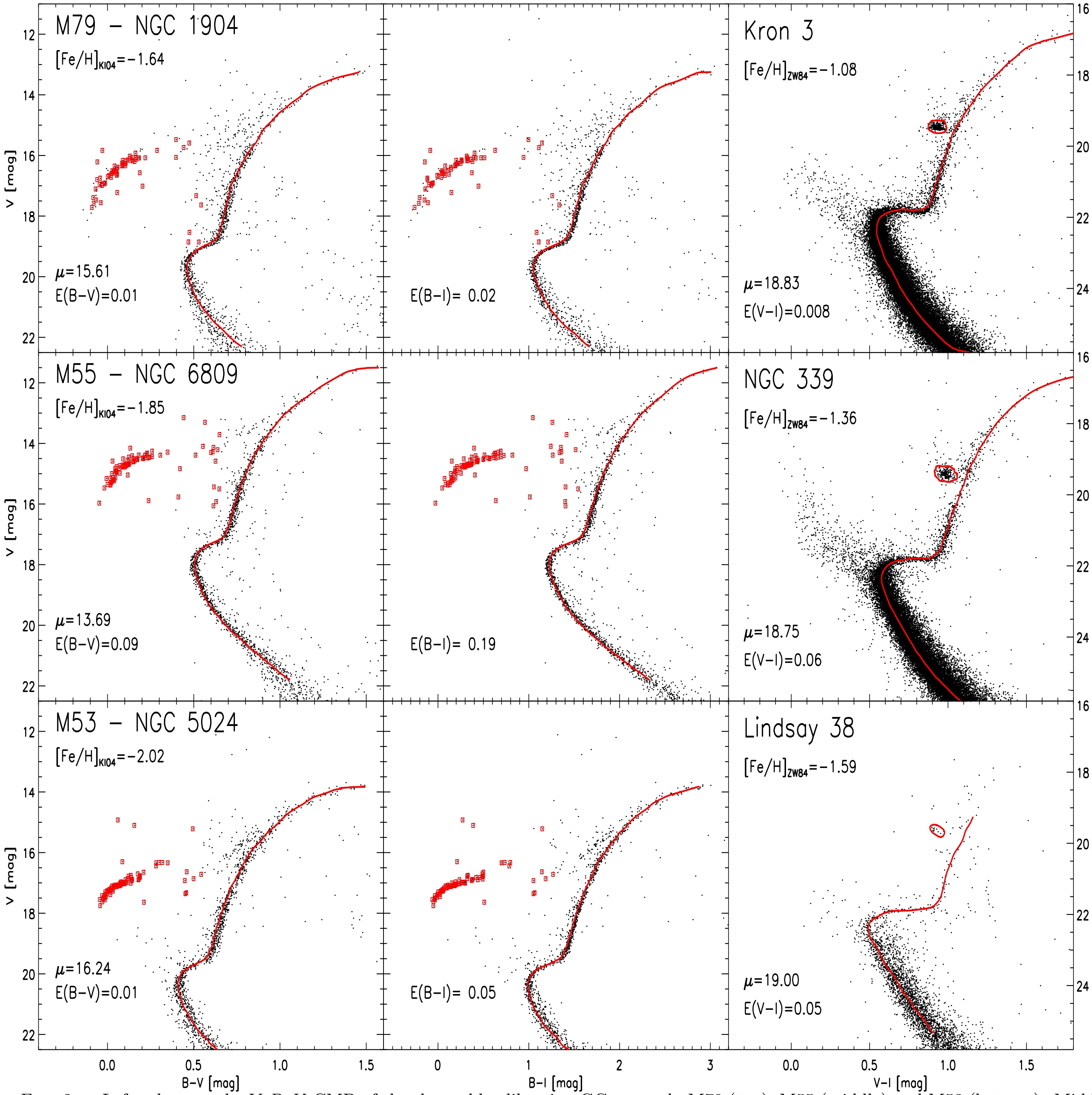

Fig. 2.— Left column – the V, B–V CMD of the three old calibrating GCs, namely M79 (top), M55 (middle) and M53 (bottom). Middle column – same as the left, but for the V, B–I CMD. Right column – the V, V–I CMD of the three intermediate-age SMC calibrating clusters, namely Kron 3 (top), NGC 339 (middle) and Lindsay 38 (bottom). The red lines display the ridge lines, the red squares mark old HB stars and the red oval the contour of RC stars. The iron abundance, the distance modulus, and the reddening are also labeled.

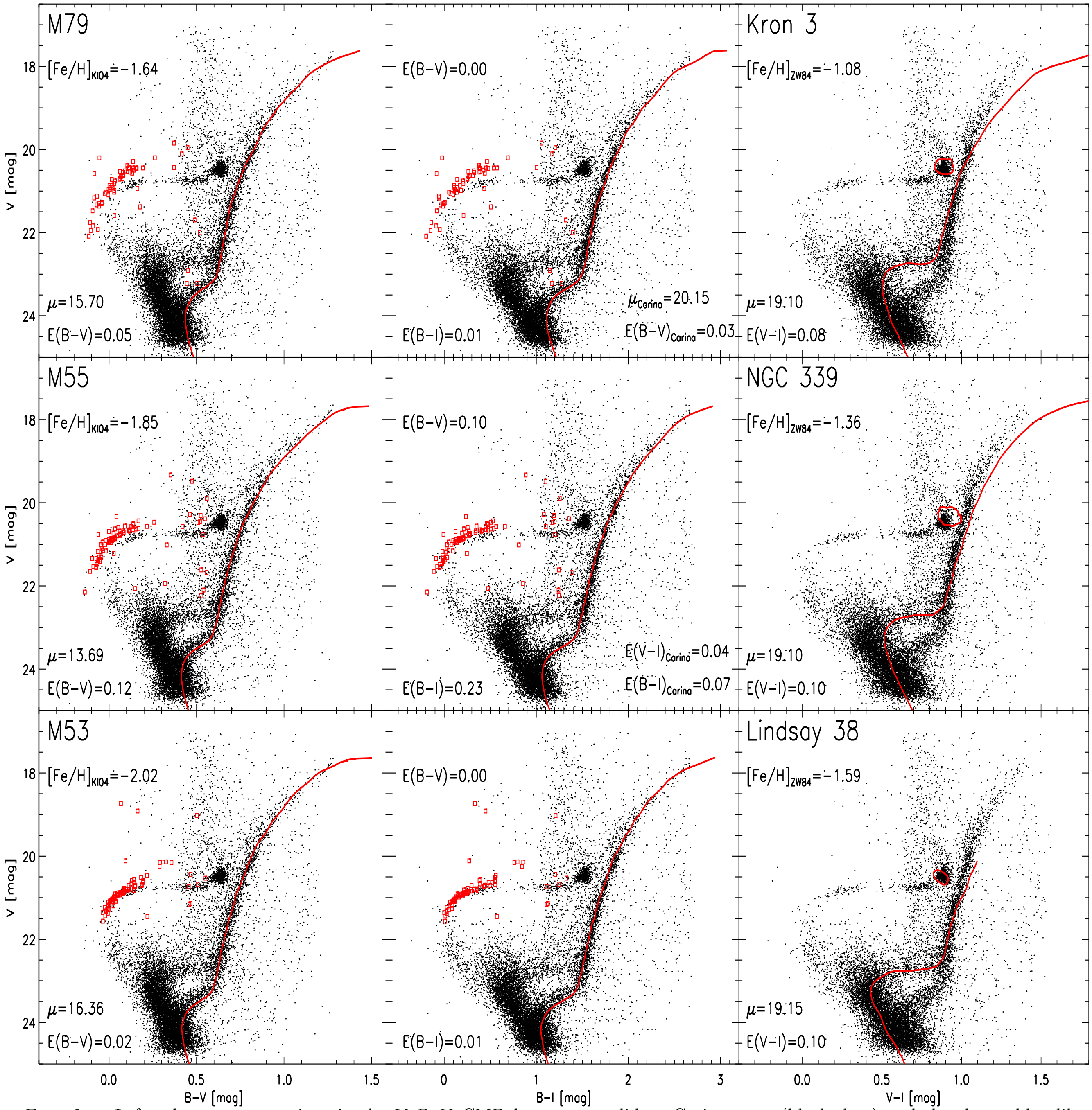

FIG. 3.— Left column – comparison in the $V, B–V$ CMD between candidate Carina stars (black dots) and the three old calibrating GCs, namely M79 (top), M55 (middle) and M53 (bottom). The distance modulus and the reddening adopted to overlap the SGB of old GCs with the SGB of Carina are labelled. Middle column – same as the left, but in the $V, B–I$ CMD. Right column – comparison in the $V, V–I$ CMD between Carina stars and the three intermediate-age SMC calibrating clusters, namely Kron 3 (top), NGC 339 (middle) and Lindsay 38 (bottom). The distance modulus and the reddening adopted to overlap the SGB of intermediate age SMC clusters with the SGB of Carina are labelled.

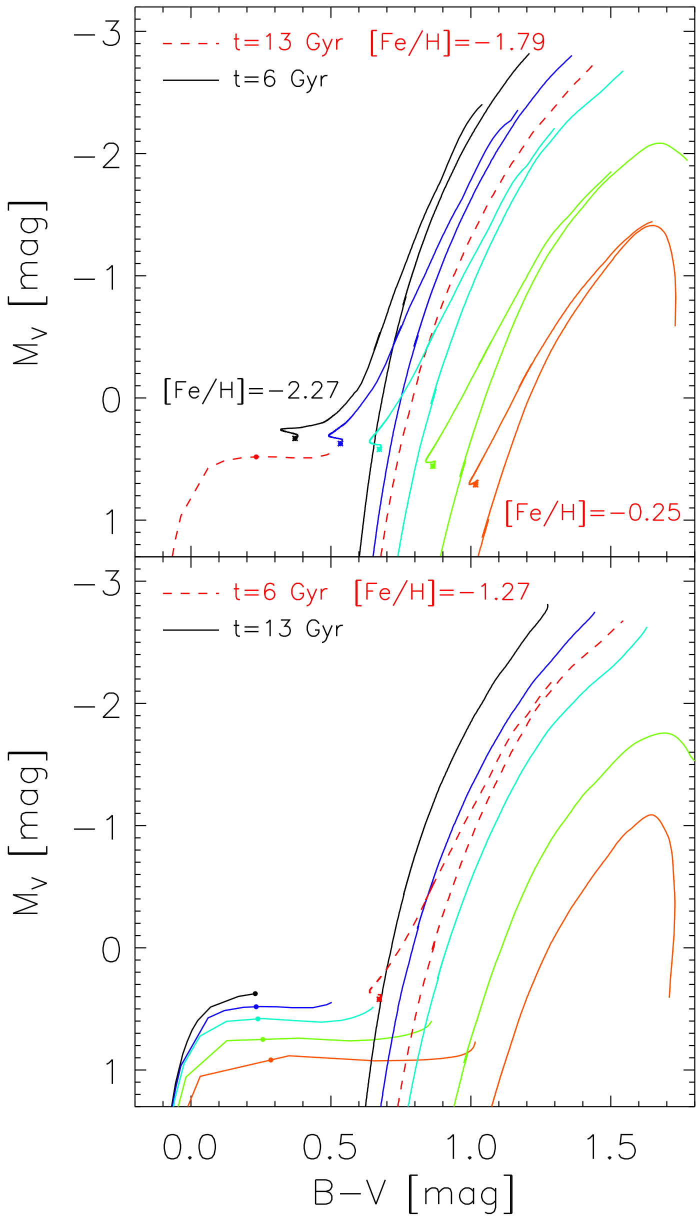

FIG. 4.— Top – cluster isochrones in the $V, B–V$ CMD at fixed age (6 Gyr) and for a broad range of chemical compositions (BaSTI database). The vertical red dashed line shows the isochrone for an old (13 Gyr), metal-poor ([Fe/H]=–1.79 dex) stellar structure together with its ZAHB. The colored lozenges mark the RC color, while the red square marks the middle of the RR Lyrae instability strip ($\log T_e$=3.85). Bottom – cluster isochrones in the $V, B–V$ CMD at fixed age (13 Gyr) and for a broad range of chemical compositions (BaSTI database). The vertical red dashed line shows the isochrone for an intermediate age (6 Gyr), metal-intermediate ([Fe/H]=–1.27 dex) stellar structure together with its He-burning phases. The symbols are the same as in the top panel.

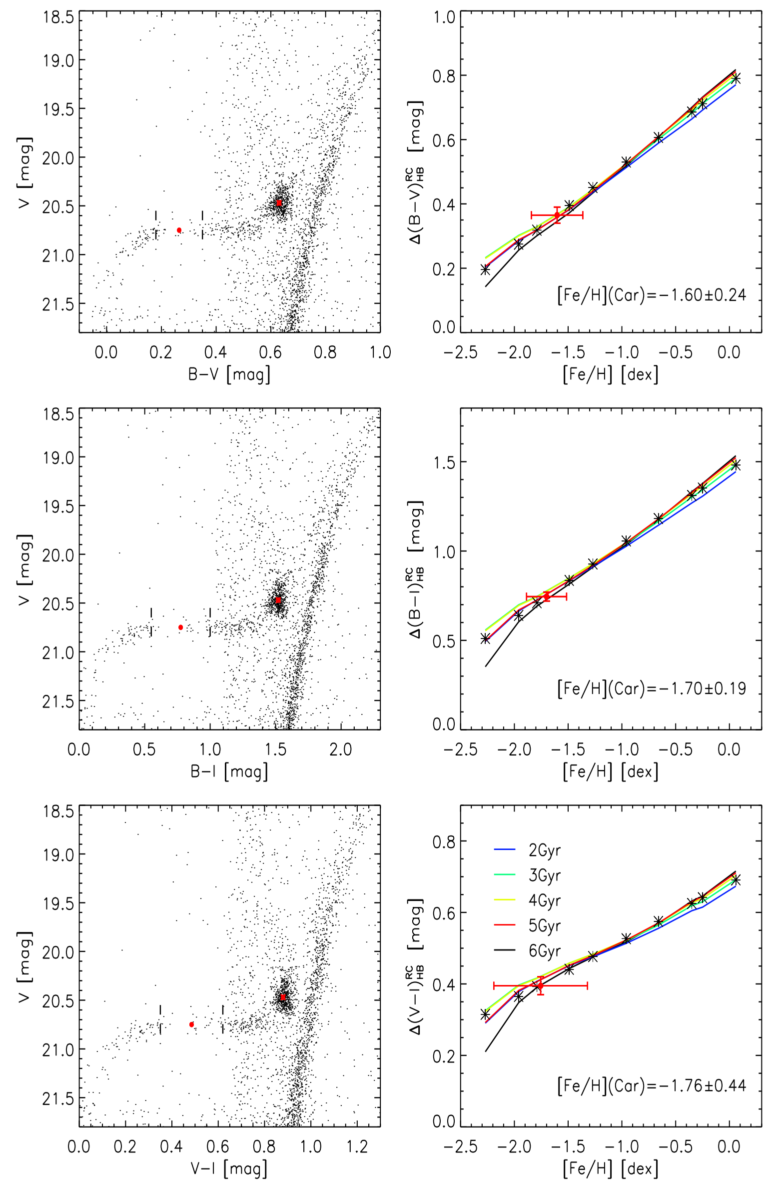

FIG. 5.— Left column – zoom across the RC and old HB region of Carina in the $V, B–V$ (top), $V, B–I$ (middle) and in the $V, B–I$ (bottom) CMD. The red circle marks the position of the middle of the RR Lyrae instability strip and the red asterisk marks the position of the peak of RC stars. Right column – Predicted difference in $B–V$ (top), in $B–I$ (middle) and in $V–I$ (bottom) colors between the middle of the RR Lyrae instability strip and the peak of RC stars as a function of iron abundance. Lines of different colors display predictions for different ages of intermediate-mass stars (see labeled values). The black asterisks mark the BaSTI grid points. The red dots display Carina, while the error bars the uncertainties affecting the difference in color and the metallicity estimate.

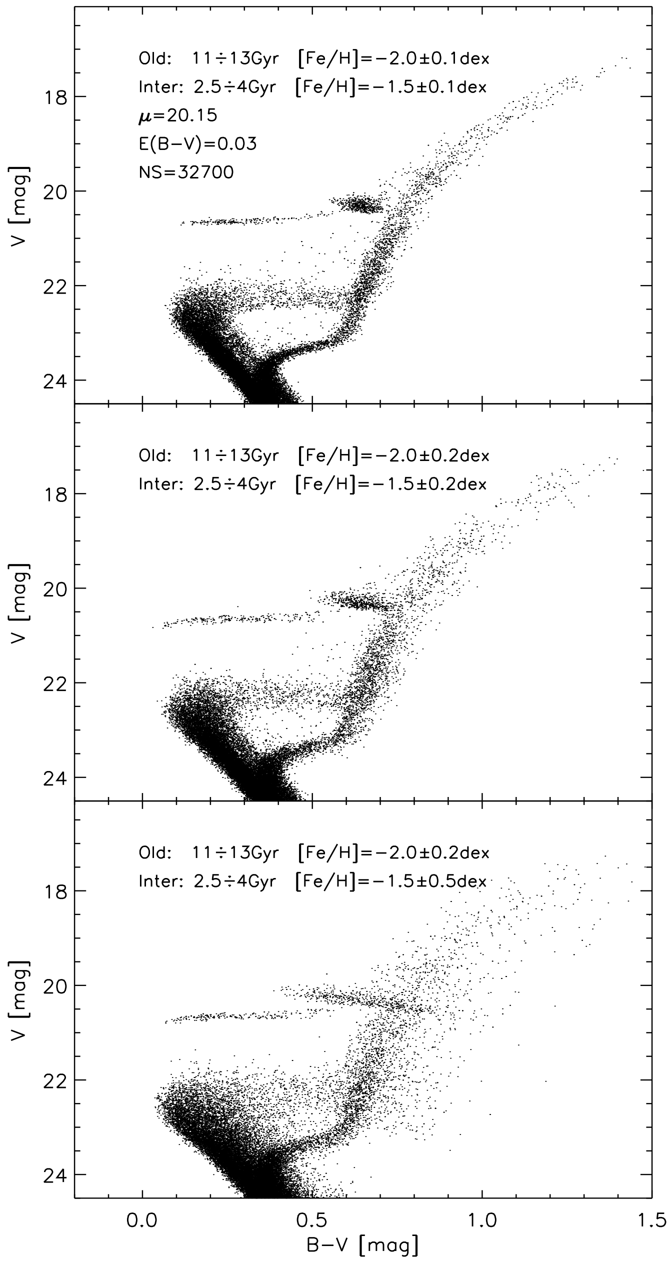

Fig. 6.— Top – synthetic $V, B–V$ CMD of Carina. The CMD was constructed by assuming two star formation episodes, with ages of 11÷13 Gyr for the old and of 2.5÷4 Gyr for the intermediate-age stellar component (Monelli et al. 2003). The two star formation episodes include the same fraction of stars and have a mean metallicity of [Fe/H]=–1.5 and of –2.0 dex, respectively. The spread in metallicity is ± 0.1 dex for both the intermdiate and the old sub-population. Intrinsic photometric error was added using a Gaussian with a mean equal to 0.02 mag. Middle – same as the top, but the synthetic CMD was constructed assuming a spread in metallicity of ± 0.2 dex for the old and the intermdiate-age sub-population. Bottom – same as the middle, but the synthetic CMD was constructed assuming a spread in metallicity of ± 0.5 dex for the intermdiate-age sub-population.